

RESEARCH

Open Access



Critical role of Oas1g and STAT1 pathways in neuroinflammation: insights for Alzheimer's disease therapeutics

Zhixin Xie^{1†}, Linxi Li^{2†}, Weizhong Hou^{1†}, Zhongxi Fan³, Lifan Zeng³, Limin He⁴, Yunxiang Ji², Jingbai Zhang², Fangran Wang², Zhou Xing^{2*}, Yezhong Wang^{2*} and Yongyi Ye^{2*} 

Abstract

Background Alzheimer's disease (AD) has a significant impact on an individual's health and places a heavy burden on society. Studies have emphasized the importance of microglia in the progression and development of AD. Interferon responses and Interferon-stimulated genes (ISGs) significantly function in neuroinflammatory and neurodegenerative diseases involving AD. Therefore, further exploration of the relationship among microglia, ISGs, and neuroinflammation in AD is warranted.

Methods Microglia datasets from the GEO database were retrieved, along with additional microglia RNA-seq data from laboratory mice. Weighted Correlation Network Analysis was used on the training dataset to identify gene co-expression networks. Genes from the black module were intersected with interferon-stimulated genes, and differentially expressed genes (DEGs) were identified. Machine learning algorithms were applied to DEGs, and genes selected by both methods were identified as hub genes, with ROC curves used to evaluate their diagnostic accuracy. Gene Set Enrichment Analysis was performed to reveal functional pathways closely relating to hub genes. Microglia cells were transfected with siRNAs targeting Oas1g and STAT1. Total RNA from microglia cells and mouse brain tissues was extracted, reverse-transcribed, and analyzed via qRT-PCR. Proteins were extracted from cells, quantified, separated by SDS-PAGE, transferred to PVDF membranes, and probed with antibodies. Microglia cells were fixed, permeabilized, blocked, and stained with antibodies for STAT1, then visualized and photographed.

Results Bioinformatics and machine learning algorithms revealed that Oas1g was identified as a hub gene, with an AUC of 0.812. Enrichment Analysis revealed that Oas1g is closely associated with interferon-related pathways. Expression of Oas1g was validated in AD mouse models, where it was significantly upregulated after microglial activation. Knockdown experiments suggested siOas1g attenuated the effect of siSTAT1, and the expressions of STAT1

[†]Zhixin Xie, Linxi Li and Weizhong Hou contributed equally to this work and share first authorship.

*Correspondence:

Zhou Xing
zhou_xing2024@126.com
Yezhong Wang
wangyezhong@gzhmu.edu.cn
Yongyi Ye
yeyongyi@gzhmu.edu.cn

Full list of author information is available at the end of the article



© The Author(s) 2025. **Open Access** This article is licensed under a Creative Commons Attribution-NonCommercial-NoDerivatives 4.0 International License, which permits any non-commercial use, sharing, distribution and reproduction in any medium or format, as long as you give appropriate credit to the original author(s) and the source, provide a link to the Creative Commons licence, and indicate if you modified the licensed material. You do not have permission under this licence to share adapted material derived from this article or parts of it. The images or other third party material in this article are included in the article's Creative Commons licence, unless indicated otherwise in a credit line to the material. If material is not included in the article's Creative Commons licence and your intended use is not permitted by statutory regulation or exceeds the permitted use, you will need to obtain permission directly from the copyright holder. To view a copy of this licence, visit <http://creativecommons.org/licenses/by-nc-nd/4.0/>.

and p-STAT1 were elevated. siOas1g could reverse the effect of siSTAT1, indicating that Oas1g potentially regulates the ISGs through the STAT1 pathway.

Conclusion We demonstrated that Oas1g was identified as a hub ISG in AD and can downregulate the activation of IFN- β and STAT1, reducing the expression of ISGs in neuroinflammation. Oas1g might potentially be a beneficial candidate for both prevention and treatment of AD.

Keywords Alzheimer's disease, Oas1g, WGCNA, Interferon-stimulated genes, Neuroinflammation, Machine learning

Introduction

AD was prevalent among more than 55 million individuals worldwide in 2024, which was estimated to rise to 152 million by 2050 [1]. As a progressive neurodegenerative disease, AD has a significant impact on an individual's health and quality of life. Elderly patients aged 65 years and older survive only 4 to 8 years after the diagnosis of AD on average [2].

AD is pathologically defined by senile plaques and intracellular neurofibrillary tangles (NFTs), comprising amyloid-beta (A β) aggregation and hyperphosphorylated Tau protein [3].

In addition to these hallmark features, neuroinflammation is considered a critical component in the development of cognitive impairments in AD [4]. This neuroinflammation is not simply a secondary event caused by the formation of senile plaques or tau aggregation but also actively contributes to the progression of AD [5]. Furthermore, recent genome-wide association studies suggested that neuroinflammation is a genetic risk factor for the initiation and progression of AD [6]. Microglia are the main players in neuroinflammation. They can clear A β and remove harmful substances through microglial scavenger receptors, phagocytosis, and extracellular degradation of A β -degrading enzymes [7]. Long-term activation of microglia and subsequent secretion of pro-inflammatory factors result in structural and functional changes. These changes worsen neuronal degeneration during the neuroinflammatory response [5]. A postmortem analysis of AD patients' brains also revealed that reactive microglia are found colocalized with amyloid plaques [8].

Interferon (IFN) response is a crucial element in the neuroinflammatory network of AD [9]. Type I IFN response in microglia mediates the activation of microglia and synaptic loss in the early stages of beta-amyloidosis [9]. Increased expression of IFNAR and elevated Type I IFN signaling lead to enhanced synaptic pruning functions in DS microglia, contributing to the progression of AD [10]. IFN-responding microglia have been identified in subpopulations of microglia from single-cell RNA-seq studies on the AD brain [11]. Interferon-stimulated genes (ISGs) are a group of genes induced during an response that defend against viruses, inhibit cell proliferation, and promote adaptive immunity [12]. In an AD

model, activated microglia expressing ISGs were found surrounding A β plaques that contained nucleic acids and accumulating age-dependently [12]. While most studies have concentrated on ISGs in the immunological response to IFN, the regulation of ISGs in AD remains unclear [13]. This gap underscores the necessity of investigating how ISGs are regulated in AD-related neuroinflammation, which is the focus of this study.

As a branch of artificial intelligence, machine learning (ML) is widely used in the fields of biomarker selection, disease diagnosis and prognosis prediction, drug development and repurposing [14, 15]. By constructing analytical models, key influencing factors are predicted or identified from present datasets, which can be further used to develop highly sensitive and accurate prognostic prediction models, diagnostic methods, or screen effective drugs [16, 17]. Two high performance machine learning methods, support Vector Machines-Recursive Feature Elimination algorithm (SVM-RFE) and Lasso regression analysis were used to screen Hub genes in this study.

Network-based analysis is widely used in biological fields such as signature gene or molecular recognition, drug repurposing and data visualization [18–20]. Among them, weighted correlation network analysis (WGCNA) is a web-based systems biology approach that analyzes patterns of correlation between genes in various samples and is able to identify gene modules that are highly associated with disease to identify potential biomarkers or therapeutic targets [19].

Our study aims to identify the hub ISGs and offer clues for important pathological mechanisms in AD. In our research, we executed a series of experiments to explore the genetics of AD (summarized in Fig. 1). We applied machine learning and WGCNA to pinpoint the hub ISGs. Subsequently, we investigated its role in the interferon-related pathway through Gene Set Enrichment Analysis. Finally, in vitro experiments as well as in vivo experiments were conducted to validate our results. Our study indicates that Oas1g functions as a hub ISG in AD, potentially downregulating the activation of IFN- β and STAT1, thereby reducing the expression of ISGs involved in neuroinflammation. These findings further elucidate the pathophysiological mechanisms of AD, reinforce the link between ISGs and AD, and may provide potential

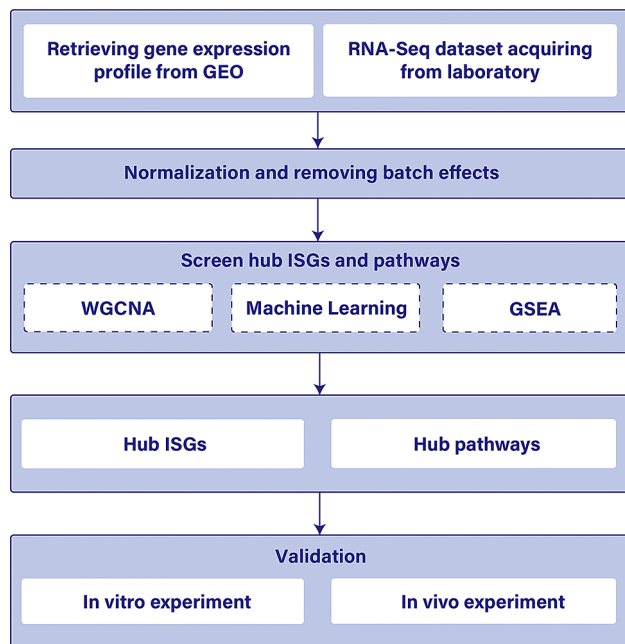


Fig. 1 The workflow to screen hub ISGs of AD in this study

biomarkers or therapeutic targets for the diagnosis and treatment of AD.

Materials and methods

Dataset acquisition

Our selection criteria were to include RNA-seq datasets of microglia from various AD-related pathotypes and wild-type controls. Sequencing data of microglia samples of AD mouse were screened from the GEO database, and the GSE129296, GSE158153, and GSE181903 datasets were filtered and downloaded. Detailed information is shown in the Supplementary Table S1. The GSE129296 dataset contains microglia RNA-seq data from 23 mice (11 samples from mice cultured for three months and 12 samples from mice cultured for 12 months). Data from 12-month-old mice were enrolled and contained 4 wild-type, 4 TAU pathotypes, and 4 APP pathotypes. The GSE158153 dataset contains microglia RNA-seq data from 30 mice, of which 10 wild-type and 10 methoxy-X04-negative APP pathotypes were screened. The GSE181903 dataset contained 6 microglia RNA-seq data containing 3 wild-type and 3 TAU pathotypes. In addition, microglia RNA-seq data from 6 mice (containing three wild-type and 3 LPS pathotype mice) were obtained in the laboratory and deposited to the GEO database with accession number GSE261007. GSE129296 and microglia RNA-seq data from mice obtained in the laboratory (GSE261007) were combined into one training dataset. GSE158153 and GSE181903 were combined into a separate validation dataset. The specific data set can be found in online repositories and Supplementary Table S1.

Data processing

After acquiring the training and validation datasets, the gene expression matrixes were normalized via the normalize BetweenArrays method in the R package “limma”. The acquired datasets were transformed into matching gene names according to the probe numbers obtained from the platform annotation information. We learned from the literature that the “Combat” can effectively remove the batch effects caused by different sequencing platforms with high accuracy and precision, which makes the combined dataset suitable for screening biomarkers or constructing genetic signatures [21]. The “Combat” function was used to remove the batch effects and merge them into one dataset. Compared with traditional dimensionality reduction methods such as PCA, tSNE and UMAP showed greater advantages in differentiating batch effects and identifying biological groups [22]. Thus we analyzed the datasets before and after the removal of the batch effects using tSNE and UMAP to verify whether the batch effects were effectively removed in training and validation datasets, respectively. The random seed was set to 1 and perplexity was set to 6 with other default parameters. Further, the boxplots before and after the removal of the batch effects were blotted. Hierarchical cluster analysis was performed using the “hclust” function in R to distinguish the profiles of the two groups of biological samples and to remove outlier samples.

Construction of gene co-expression network

Weighted Correlation Network Analysis (WGCNA) is a systems biology method that constructs gene co-expression networks to reveal functional and co-regulatory gene relationships through shared expression patterns [23]. The merged training dataset was used to construct a co-expression network with the R package “WGCNA”. Initially, the sample clustering tree algorithm is used to filter out outliers, ensuring the stability of the co-expression network construction. The gene connections in the co-expression network exhibit a scale-free distribution, and a soft threshold function is employed to determine the optimal soft threshold β . To minimize spurious correlations and noise, the adjacency matrix is converted into a topological overlap matrix (TOM). The 1-TOM is computed as a crucial biological indicator of network interconnectivity and gene clustering distance. Next, a dynamic tree cutting algorithm is used to identify gene modules. Module eigenvalues (ME) are then calculated, and hierarchical clustering is performed. Similar modules are merged and differentiated by distinct colors. WGCNA allows us to identify genes that are associated with target traits, screen for hub genes, and obtain co-expression modules with significant biological relevance.

Differentially expressed genes

Five gene modules were obtained through the dynamic clipping module, and the black module had the highest correlation with AD among all gene modules with the most significant p-value. To further filter the hub ISGs, the gene set of the black module obtained from WGCNA analysis was overlapped with the genes in the interferon-stimulated gene datasets to obtain the intersected genes. Datasets of Interferon-stimulated genes were obtained from the online Interferome database available at <http://interferome.its.monash.edu.au/interferome/home.jsp>, where the filter criteria in the database is $|\log_{2}FC| \geq 2$. Subsequently, the intersected genes were subjected to analysis for differentially expressed genes (DEGs) using the R package “limma”. The cut-off value was set to $|\log_{2}FC| \geq 1$ and the adjusted p-value was < 0.05 to filter statistically significant DEGs in each dataset. The visualization of DEGs was performed with the “pheatmap” package utilizing default settings. Volcano plots, created using ggplot2 in R, were employed to illustrate the DEGs, based on $\log_{2}(\text{Fold Change})$ and $-\log_{10}(\text{p value})$.

Identification of hub genes using machine learning

Lasso is a machine learning algorithm that utilizes L1 regularized linear regression models, which is widely used for screening gene expression data to improve prediction accuracy [24]. The support Vector Machines-Recursive Feature Elimination (SVM-RFE) algorithm is a machine learning method that filters relevant features and removes relatively unimportant feature variables to improve the classification accuracy of datasets more effectively [25, 26]. We used the gene set of DEGs for Lasso and SVM-RFE analyses, respectively, and subsequently took the intersection of the two gene sets to filter out the hub ISGs. For both LASSO regression and SVM-RFE, the seed setting was 3. A LASSO regression model was developed using the “glmnet” package. In parallel, the SVM-RFE model was created to identify the feature genes. This was executed via the R package “e1071,” “kernlab,” and “caret”. Furthermore, we assessed the accuracy of machine learning by calculating receiver operating characteristic (ROC) curves and measuring the area under the curve (AUC) in the validation set. The ROC curve has been extensively utilized in medical fields to assess the efficacy of deep learning diagnostic techniques. The AUC was calculated to reflect the model’s ability to differentiate between positive and negative instances. AUC values range from 0 to 1, where higher values signify superior model performance [27]. Genes screened by overlapping Lasso and SVM-RFE analyses were used to plot boxplot and ROC diagnostic curves. The boxplot was plotted by the R package “ggpubr” and the ROC diagnostic curve was created by the R package “pROC”.

Gene set enrichment analysis

Gene set enrichment analysis (GSEA) was employed to assess the distribution patterns of genes in predefined gene sets within a gene list that is ordered based on their phenotypic relevance to determine their phenotypic contribution [24]. GSEA analysis for the training datasets was performed using “GSEA” function in the R package “ClusterProfiler”. Predefined gene sets were obtained from the R package “msigdb”, which includes GO, KEGG, and immune-related datasets. The GSEA results were visualized by utilizing the gseaNb function available in the GseaVis package. The statistical significance criteria were set at default standard with $\text{Padj.} < 0.05$ and $\text{FDR} < 0.25$.

Cell cultures and treatment

The BV2 cell seeding density was maintained between 70% and 80%. The cells were cultured in a high-glucose medium (Gibco) supplemented with 10% fetal bovine serum (ExCell Bio) and incubated at 37 °C with 5% CO₂. To induce microglial activation, BV2 cells were exposed to different durations (3 h, 6 h, 12 h, 24 h) and concentrations (200ng/ml, 500ng/ml, 1000ng/ml) of lipopolysaccharide (LPS).

Isolation and culture of mouse primary microglia

Primary microglial cells were extracted from the cerebral cortex of newborn C57BL/6 mice aged 0–2 days. The brain tissue was dissected, and both hemispheres were isolated. The meninges were removed, and the tissue was finely minced using microscissors on an ice surface. The tissue fragments were then placed in Accutase digestion enzyme (Sigma) with Deoxyribonuclease I (Invitrogen) and incubated at 37 °C for 30 min with gentle shaking every 10 min. The tissue suspension was filtered and centrifuged. The cell pellet was resuspended, and the cells were seeded into culture flasks pre-coated with poly-L-lysine (Sigma). Primary microglial cells were cultured in high-glucose medium (Gibco) supplemented with 20% serum (ExCell Bio), 1% penicillin-streptomycin (Gibco), and maintained in an incubator at 37 °C with 5% CO₂. Once the cells grew, gentle shaking T-75 flasks at 230 rpm at a temperature range of 18 °C to 26 °C for over 3 h. After this incubation, cells and media were collected by centrifugation at 180 rcf for 5 min, separating microglial cells from astrocytes. The cells were centrifuged, resuspended, and then seeded into six-well plates for subsequent treatments.

siRNA transfection

BV2 cells were seeded into six-well plates, and when the cell density reached 60%, transfection was performed in accordance with the manufacturer’s instructions using Lipofectamine RNAiMAX (Invitrogen) to introduce the

negative control, siOas1g, and siSTAT1 into the cells. In a six-well plate, an appropriate amount of transfection reagent was added to achieve the final siRNA concentration of 50 nM.

After 24 hours of transfection, the medium was replaced with DMEM containing 10% FBS for subsequent treatments. The siRNA sequences used were as follows: Negative control :5'-UUCUCCGAACGUGUCACGUTT-3'; Oas1g (si1: 5'- GGUCAUGGUAGUAUCAAUATT-3'; si2: 5'- CTCATCTGGGAATGTACCT-3') Stat1 (si1:5'- ATGCATCTTACTGAAGGTGAA -3'; si2:5'-ATGAGTTGGTTTAATATATAT-3'). These siRNA sequences were synthesized by GenePharma Biotechnology (Shanghai, China) and RiboBio (Guangzhou, China).

RNA isolation and quantitative real-time PCR

Total RNA was extracted from BV2 cells and mouse brain tissues using RNAiso Plus reagent (Takara, Japan), and the RNA concentration was measured by NanoDrop ND1000 Spectrophotometer. The cDNA was reverse synthesized using ReverTra Ace qPCR RT Master Mix with gDNA Remover (TOYOBO, Japan) according to the manufacturer's instructions. After that, the reaction system was set up using TB Green® Premix Ex Taq™ II (TaKaRa, Japan) according to the directions, and qRT-PCR was performed in a Roche Light Cycler 480II System (Roche). The relative gene expression levels were determined utilizing the 2- $\Delta\Delta$ Ct method with β -actin serving as the internal reference control. The primer sequences were designed by Sangon Biotech and synthesized by BGI. All primer sequences are shown in the Supplementary Table S2.

Western blot

The collected cells were mixed with RIPA buffer (Beyotime Biotechnology) containing protease and phosphatase inhibitors. The entire mixtures were then incubated on ice for 30 min. The final products were then centrifuged for 5 min at 12,000 rpm at 4 °C before being transferred to new EP tubes. The Pierce BCA Protein Assay kit (Thermo Fisher Scientific) was used to measure the protein concentration in accordance with the reagent instructions. Protein samples were combined in a 4:1 ratio with 5x Loading buffer (NCM Biotech) and then boiled for 10 min. 10% SDS-PAGE gels were used to load equal amounts of protein, which were then electrophoresed and transferred onto PVDF membranes (MilliporeSigma). To block the nonspecific bindings, the membranes were subsequently blocked with 5% non-fat milk (Sangon Biotech) in TBS containing Tween 20 (TBST) for an hour at room temperature. Primary antibodies including STAT1 (1:1000, CST, 14994), Phospho-Stat1 (1:1000, CST, 7649), and β -actin (1:1000, ZSGB-BIO, TA-09) were incubated overnight at 4 °C.

The membranes underwent three 10-minute washes with TBST at room temperature to remove unbound primary antibodies and then were incubated with horseradish peroxidase-conjugated secondary antibodies (1:10000, Jackson, 111-035-003, 115-035-003) for 1 h. And images were taken on a chemiluminescence imager (ChemiScope 6300, Clinx Science Instruments) using HRP Substrate Luminol Reagent (Millipore). Finally, the banding results were analyzed using Image J software (US National Institutes of Health) and signals were normalized to β -Actin.

Immunofluorescence and image analysis

BV2 cells were washed with PBS and subsequently fixed using a 4% paraformaldehyde solution for a duration of 15 min at room temperature. After being fixed, the cells were washed three times with PBS for 5 min each. To facilitate antibody penetration, the cells were incubated with 0.3% Triton X-100 at room temperature for 20 min. Subsequently, the cells were cultured in goat serum for an hour. STAT1 (1:200, CST, 14994), the primary antibody, was incubated at 4 °C for an entire night. Following three 10-minutes washes with PBS, the secondary antibody (1:200 dilution, CST, 4412) was subjected to an incubation period of 1 h at room temperature away from light. All the antibodies were diluted by Antibody Dilution Buffer (Beyotime, P0277). Using an inverted fluorescent microscope (IX73, Olympus), the cells were then photographed after being put in an anti-fade mounting media containing DAPI (ZSGB-BIO, ZLI-9557). Fluorescence intensity were quantified by using Image J software (US National Institutes of Health).

Statistical analysis

All data was analyzed and processed using Graphpad Prism 9.0. The mean \pm standard deviation was used to express all data. One-way ANOVA was used to assess significant differences between several groups, and the two-tailed Student's t-test was applied to examine distinctions between the two groups. A p-value below 0.05 was considered to indicate statistical significance (* $p < 0.05$, ** $p < 0.01$, *** $p < 0.001$).

Results

Processing of gene expression data

We performed batch effect removal and evaluation on the training as well as validation datasets, respectively. In the training dataset, the UMAP plot and tSNE plot showed the distribution characteristics of GSE129296 (batch 1) and the lab-obtained dataset (batch 2) before and after removing the batch effect (Supplementary Figure S1A, B). After removing batch effects, the data distribution converged in the same group and was clearly distinguishable from the control and AD groups. Compared to the plot before batch effect removal (Supplementary

Figure S1C), the hierarchical cluster plots after batch effect removal (Supplementary Figure S1D) clearly distinguished samples from the control and AD groups and clustered the samples in the same groups together. The boxplots of two datasets without and with batch effect removal were shown in Supplementary Figures S1E and S1F. The above results suggested that the batch effect in the training dataset was removed, enhancing the reliability of subsequent analysis results. In the validation dataset, based on the cluster trees (Supplementary Figure S2A), 2 abnormal samples in the GSE158153 dataset were excluded with a branch cut height of 130. Compared to the distribution before batch effect removal, data distribution after the removal of batch effects converged in the same group and clearly distinguished samples from the control and AD groups (Supplementary Figure S2B, C). Supplementary Figures S2D and E show the boxplot of the training set before and after the removal of the batch effect. The above results suggested that the batch effects in the validation dataset were removed, making the subsequent analysis results more reliable.

Construction of weighted gene co-expression network and identification of critical modules

A WGCNA network was constructed to identify hub genes for AD using the merged training dataset. We built a weighted neighbor-joining matrix and defined a correlation that shows strong relationships between genes. To adhere to the scale-free assumption of the constructed biological networks, a soft thresholding parameter (β) value of 14 was chosen based on WGCNA guidelines (Fig. 2A). Subsequently, module characteristic genes, which represent the comprehensive gene expression profiles of each module, were calculated and clustered based on their correlations (Fig. 2B). Five gene modules were identified by dynamically clipping and merging similar modules, which may be associated with the development of AD. Based on module-clinical feature correlation heatmap analysis (Fig. 2C and D), the black module exhibited the highest correlation with AD among all the gene modules ($cor = 0.84, p = 1e-05$), indicating a statistically significant relationship. A total of 605 genes within the black module were selected for further analysis.

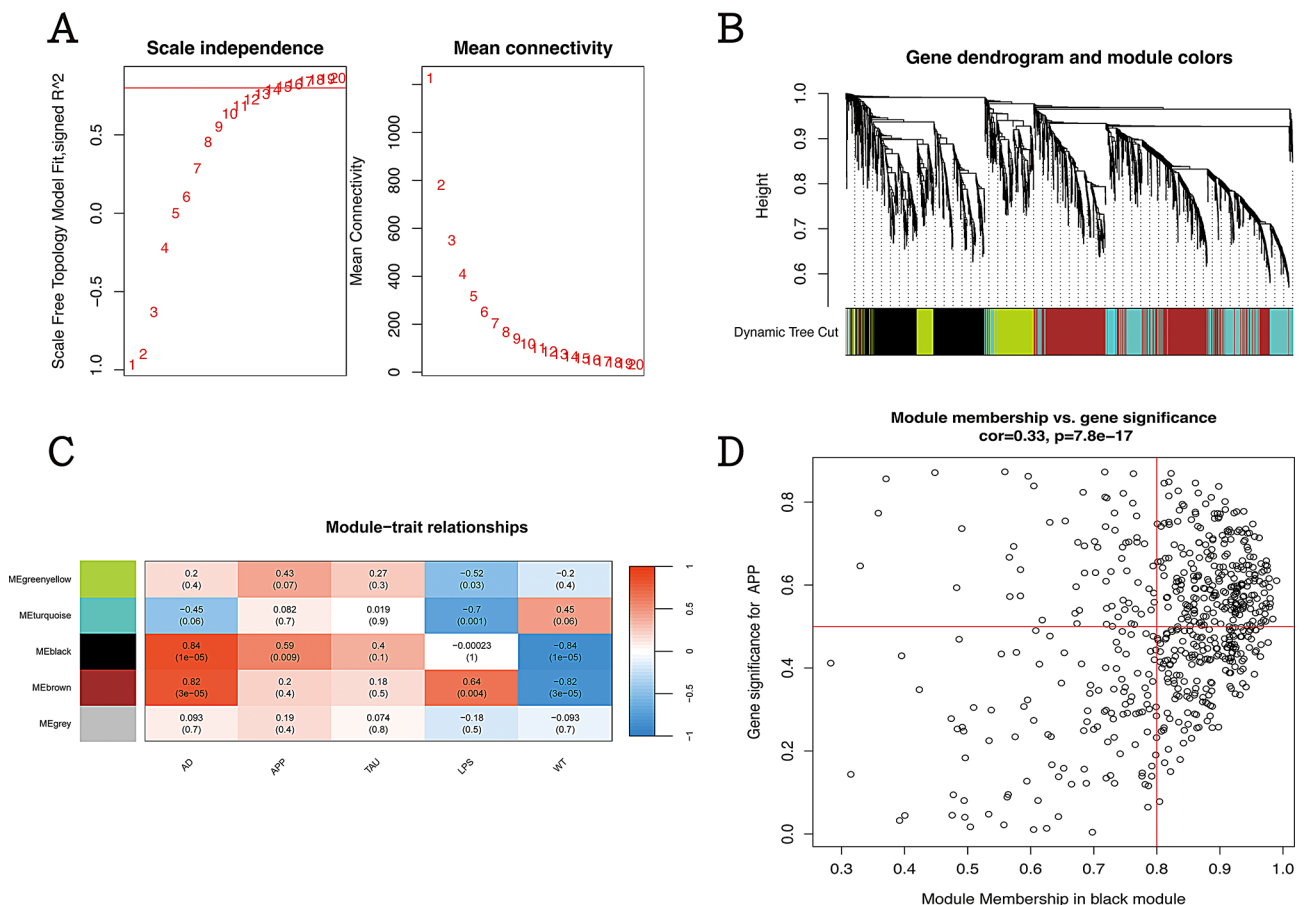


Fig. 2 Results of WGCNA analysis. (A) The mean connectivity and soft-thresholding power scale-free fit index. (B) Clustering dendrograms for genes and traits. Hierarchical clustering was utilized to generate gene clustering trees (dendrograms) from neighbor-based differences. (C) Five co-expression gene modules. The value in each cell represents the correlation coefficient and p-value. The black module was the gene module with the highest correlation with AD ($cor = 0.84, p = 1e-05$). (D) Module membership and gene significance analysis of black modules

Identification of DEGs between AD and control groups

The black module obtained from WGCNA overlapped with the interferon-stimulated genes datasets, and 510 genes used to identify DEGs were obtained. $|\log_{2}FC| \geq 1$ suggests that a gene that is differentially expressed exhibits a fold change of 2, a threshold often regarded as biologically meaningful within biological research. The adjusted p -value was <0.05 denotes statistical significance, facilitating the identification of genes that show notable differential expression across various diseases. Consequently, these established cut-off criteria assist in minimizing false positives and enhancing the reliability of the study outcomes. 209 DEGs were screened for the subsequent analysis, among which 149 DEGs were found to be upregulated, and 60 DEGs were downregulated, including up-regulated genes like *Oas1g*, *Il1rn*, and *Mnda*. These genes suggest that ISGs have a significant impact on neuroinflammation associated with AD and may serve as potential candidates for both the prevention and treatment of AD (Fig. 3).

Oas1g was screened as a hub gene based on machine learning

The 209 DEGs were screened for LASSO and SVM-RFE analysis. The LASSO analysis screened 3 genes, and the SVM-RFE analysis screened 36 genes (Fig. 4A and B). The genes screened by both were overlapped and “*Oas1g*” was screened as a hub gene (Fig. 4C). From a biological perspective, the hub gene *oas1g* plays a core regulatory role in the pathogenesis of AD and may participate in important signaling pathways or functional networks. Statistically, *oas1g* shows strong predictive power and stability in the model, significant discriminative power

and reliability in the data, and has high specificity and safety in AD neuroinflammation. Subsequently, we constructed a ROC diagnostic curve in the validation dataset to test our analysis results. The AUC of the AD diagnosis model created by *Oas1g* was 0.812, with a 95% confidence interval of 0.6324–0.9926 (Fig. 4D). The area under the ROC curve (AUC) was significantly larger than 0.5, indicating a more accurate prediction. We also validated the expression of *Oas1g* in the validation dataset. We found that the expression trend of *Oas1g* was consistent with the training dataset, and the expression of *Oas1g* in the AD group was significantly higher ($p = 0.0083$) than in the control group (Fig. 4E).

GSEA analyses revealed close associations with multiple interferon-related pathways

GSEA analysis was conducted on the merged training dataset to investigate potential signaling pathways. As shown in Fig. 5, the enrichment results indicated that interferon-related pathways were significantly enriched in the high *Oas1g* expression group ($P_{adj} < 0.05$ and $FDR < 0.25$), including “Response To Interferon Beta”, “Negative Regulation Of Type I Interferon Mediated Signaling Pathway”, “Response To Type I Interferon”, “IFN α Response”, “Interferon Response”, “Type II Interferon Signaling IFN- γ ”, “IFN β 1 Targets”, etc. GSEA results suggested that *Oas1g* may influence the function and reactivity of microglia by modulating interferon-related pathways, including both Type I and Type II interferon pathways.

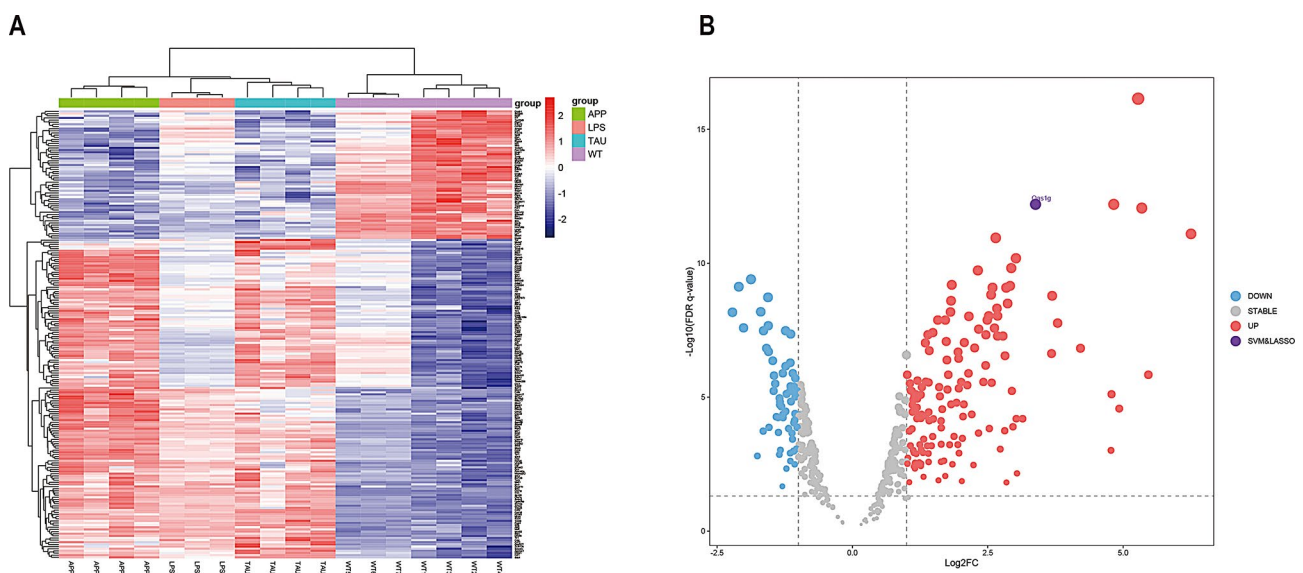


Fig. 3 Results of DEGs. (A) Heatmap of 209 DEGs. (B) DEGs between AD and control groups, where the purple scatter is the intersecting gene “*Oas1g*” for SVM-RFE and LASSO

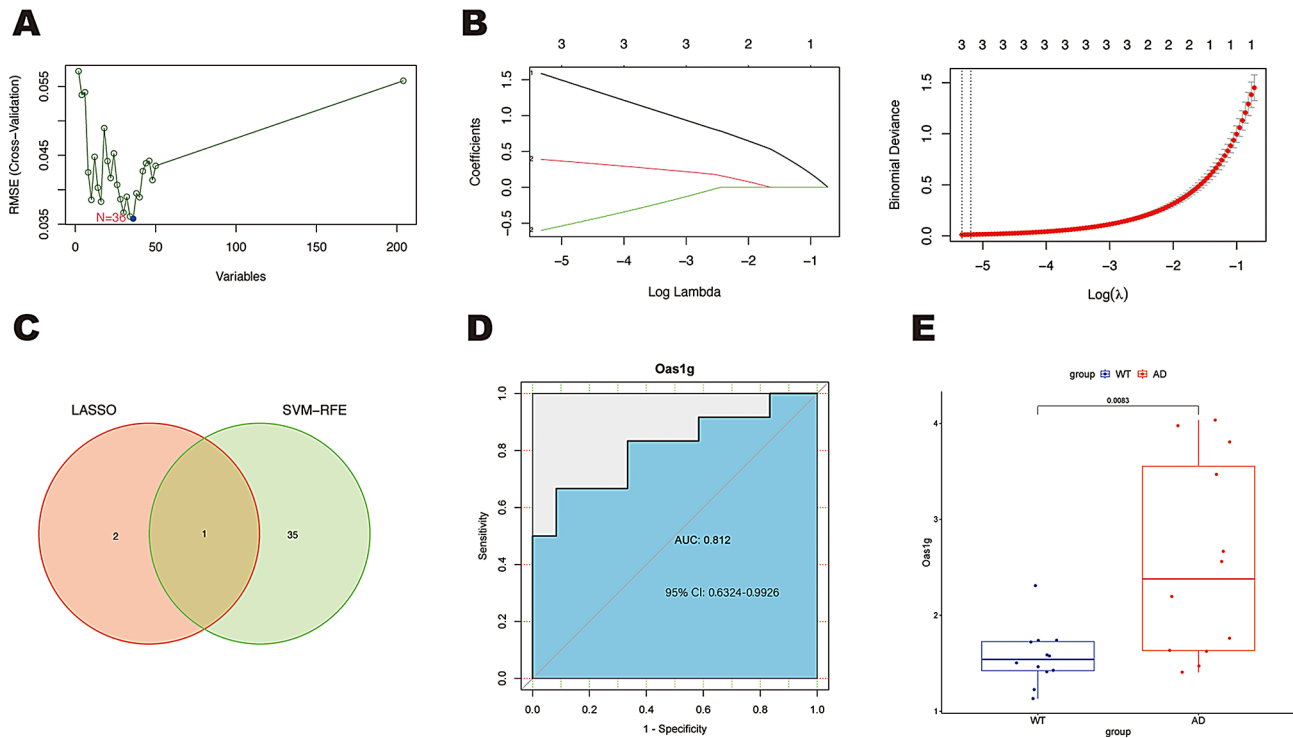


Fig. 4 Hub genes were screened using ML and validated in the validation dataset. **(A)** Employing the SVM-RFE algorithm for biomarker screening. The x-axis represents the number of feature selections, while the y-axis displays the prediction accuracy. **(B)** Screening Biomarkers Using the Lasso Algorithm. The graphic on the left displays a coefficient curve for each individual gene. In the right picture, the solid vertical lines indicate the partial likelihood of deviance. The number of genes ($n=3$) that corresponds to the lowest point of the curve is considered the most appropriate. The solid vertical lines in the right figure depict the partial likelihood of deviance, whereas the lowest point on the curve determines the ideal number of genes. **(C)** The Venn diagram demonstrates that candidate diagnostic genes are identified using SVM-RFE and Lasso algorithms. **(D)** AUC was 0.812 with a 95% CI of 0.6324–0.9926. **(E)** *Oas1g* expression was higher in AD mouse microglia than in control mouse microglia in the validation dataset ($p=0.0083$)

After microglial activation, the expression of *Oas1g* is upregulated

To further validate the expression of *Oas1g* in AD and investigate the regulatory mechanism of interferon-stimulated genes (ISGs), we initially conducted validation experiments in mice. The cortical regions of brain tissues from APP/PS1/tau transgenic mice were used to analyze *oas1g* mRNA expression levels, as these mice have been shown to closely mimic the pathological alterations seen in individuals with AD. Compared to wild-type C57BL/6 mice, we discovered that the mRNA levels of *Oas1g* in APP/PS1/tau transgenic mice were significantly higher (Fig. 6A). To verify the expression of *Oas1g* after microglial activation, we used the LPS-induced inflammation model in primary microglial cells. Treating these cells with 1000 ng/mL of LPS for 24 h led to a significant upregulation of *Oas1g* expression (Fig. 6B). Furthermore, by subjecting BV2 microglial cells to different concentrations and durations of stimulation, we observed that the mRNA levels of *Oas1g* increased in a way that was dependent on both dose and time (Fig. 6C, D). According to these findings, *Oas1g* may be a key pathogenic mechanism of AD and is linked to the disease.

Oas1g regulates ISGs via the STAT1 pathway

To investigate the influence of *Oas1g* on interferon-stimulated genes (ISGs), we employed siRNA to knock down *Oas1g* expression and subsequently applied qRT-PCR to detect the knockdown effect (Fig. 6F). After the knockdown of *Oas1g*, we observed a remarkable upregulation of IFN- β and representative ISGs expression (ISG-15, ISG-20, IFIT1, IFIT2, IFI203, IFI204, RSAD2, MX1) upon stimulating bv2 microglial cells with 1000ng/ml LPS (Fig. 6E). Following the down-regulation of *Oas1g*, a notable upregulation in the expression of STAT1 and p-STAT1 was observed through western blot and Immunofluorescence (Fig. 7A, B). Therefore, we hypothesized that the regulation of ISGs by *Oas1g* was STAT1-dependent. In order to illustrate the observed phenomena, we knocked down both *Oas1g* and STAT1 in bv2 microglia cells. Our results demonstrated that, in conditions of LPS-induced microglia activation, si*Oas1g* attenuated the effect of siSTAT1, and the expressions of STAT1 and p-STAT1 were elevated (Fig. 7C). Similarly, qRT-PCR results confirmed that si*Oas1g* could reverse the effect of siSTAT1, indicating that *Oas1g* potentially regulates the ISGs through the STAT1 pathway (Fig. 7D).

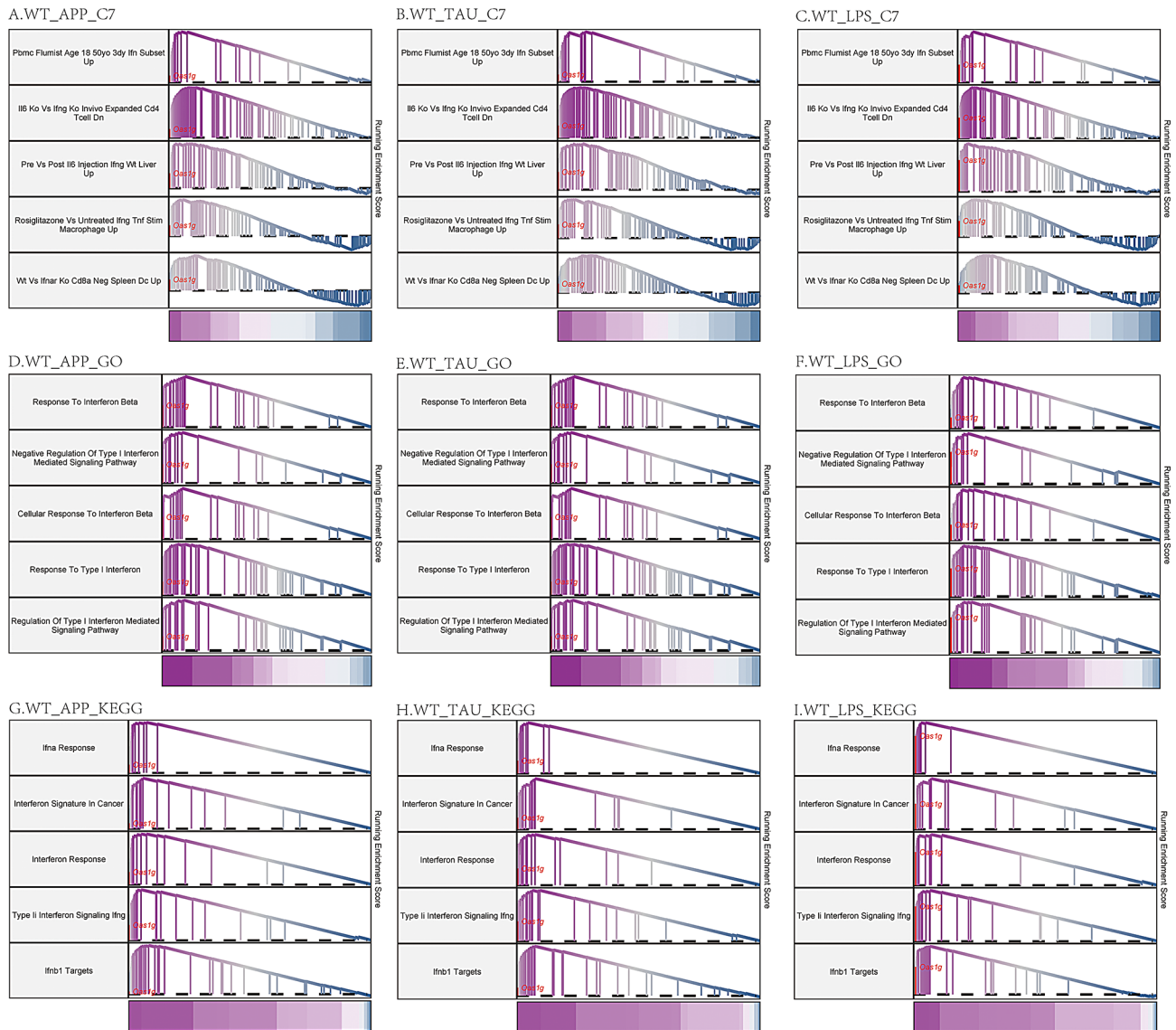


Fig. 5 Enrichment map of GSEA. **(A-C)** Enriched interferon-related pathways using the C7 immune-related dataset as a predefined gene set. **(D-F)** Enriched interferon-related pathways using the GO dataset as a predefined gene set. **(G-I)** Enriched interferon-related pathways using the KEGG dataset as a predefined gene set

Discussion

More than 55 million patients globally have been suffering from AD, which was estimated to reach 152 million by 2050 [1]. AD places a heavy burden on the family and is associated with the highest cost to society [28]. Due to the limited symptomatic treatments currently available and the slow development of disease-modifying treatments, it is critical to delve into the underlying pathophysiological mechanisms of AD [29]. Neuroinflammation is considered a vital driver in the development of cognitive deficits in AD [4]. Microglia are the main player in neuroinflammation [8], and microglial activation facilitates the production of A β and promotes the seeding of amyloid plaques [30]. Moreover, microglia

and IFN-related pathways serve as crucial mediators in the loss and dysfunction of synapses before the formation of plaques [31].

IFN response is profoundly increased and is closely associated with the severity of AD [13]. Roy et al. demonstrated that Type I IFN signaling contributes to neuroinflammation and synapse loss in AD models. By blocking Type I IFN, they observed decreased microglial activation and rescued synapse loss, suggesting a potential therapeutic avenue [12]. Similarly, Weekman et al. found that Type II IFN induced a neuroinflammatory phenotype in APP/PS1 mice and was associated with an increase in amyloid- β peptide deposition, contributing to higher levels of amyloid burden and the progression of

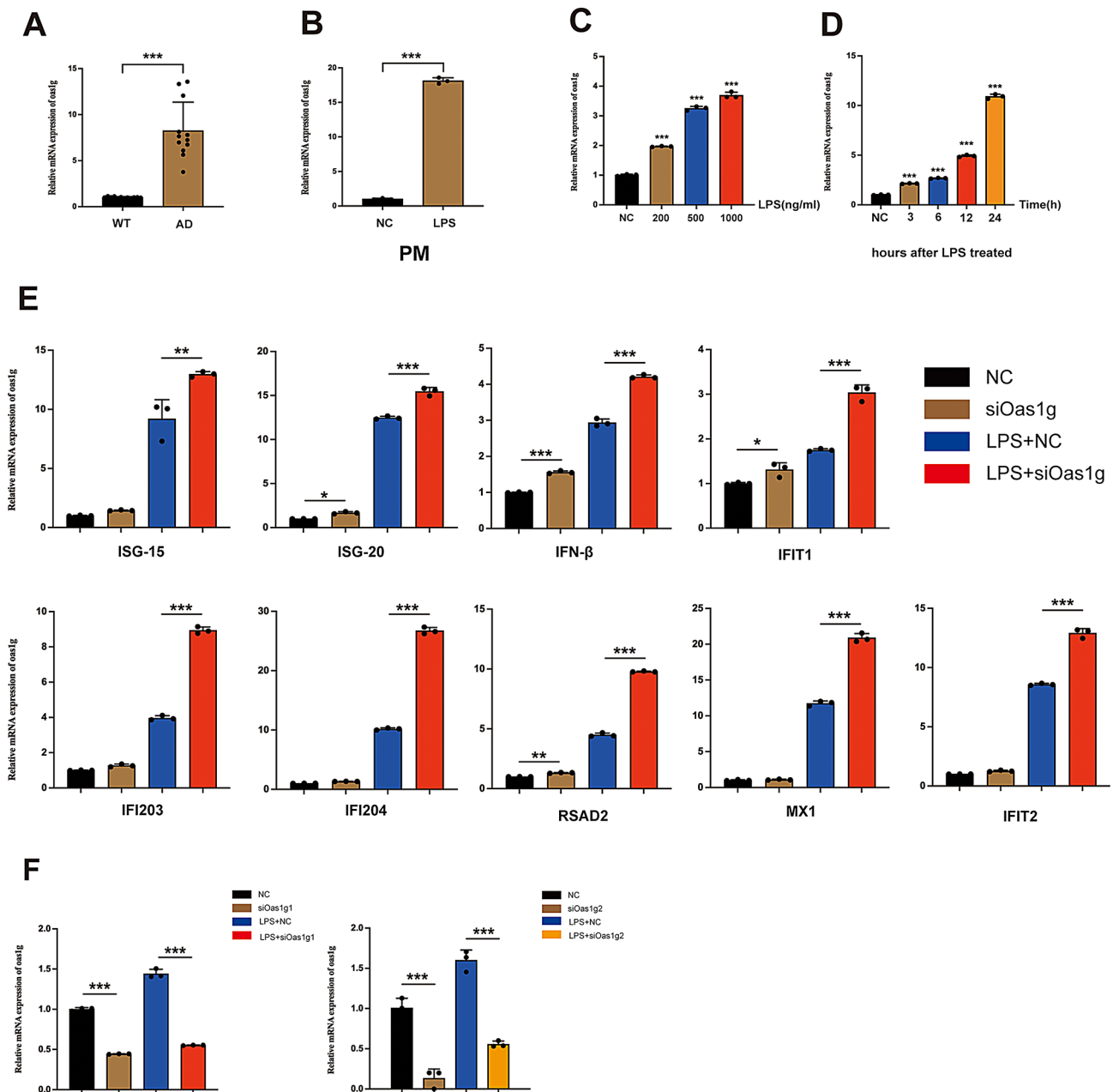


Fig. 6 The expression of ISGs in microglia demonstrates a correlation with Oas1g. **(A)** Oas1g expression level in APP/PS1/tau mouse model($n=6$); **(B)** Oas1g expression in primary microglia following LPS treatment; **(C-D)** BV2 microglial cells were treated with LPS, and then the Oas1g mRNA expression levels were detected by qRT-PCR. Oas1g was expressed in microglia cells after LPS treatment in a dose- **(C)** and time- **(D)** dependent manner. **(E)** qRT-PCR was performed to validate the expression of ISGs in BV2 microglial cells subsequent to the downregulation of Oas1g. **(F)** BV2 microglial cells were transfected with siOas1g and negative control and treated with LPS for 24 h. qRT-PCR was performed to detect the transfection efficiency. Data are expressed as mean \pm SD. (* $p < 0.05$, ** $p < 0.01$, *** $p < 0.001$)

AD [32]. Their findings indicate that Type II IFN exacerbates AD pathology, highlighting the role of IFN signaling in disease progression.

ISGs, or interferon-stimulated genes, are a group of genes induced during an IFN response [33]. Recent studies revealed that ISGs play important roles in AD and neuronal injuries. Hur et al. found that IFITM3, an ISG, enhanced the activity of γ -secretase to produce $A\beta$,

contributing to the progression of AD [34]. As a TAM receptor tyrosine kinase and ISG, AXL was screened as a regulator of microglial functions and may be used as early biomarkers of AD [35, 36]. Wang et al. revealed that ISG15 serves as a general biomarker for both acute and long-term neuronal impairment, and the upregulation of ISGs is a shared characteristic in neuronal damage, including neuroinflammation [37]. Therefore, IFN

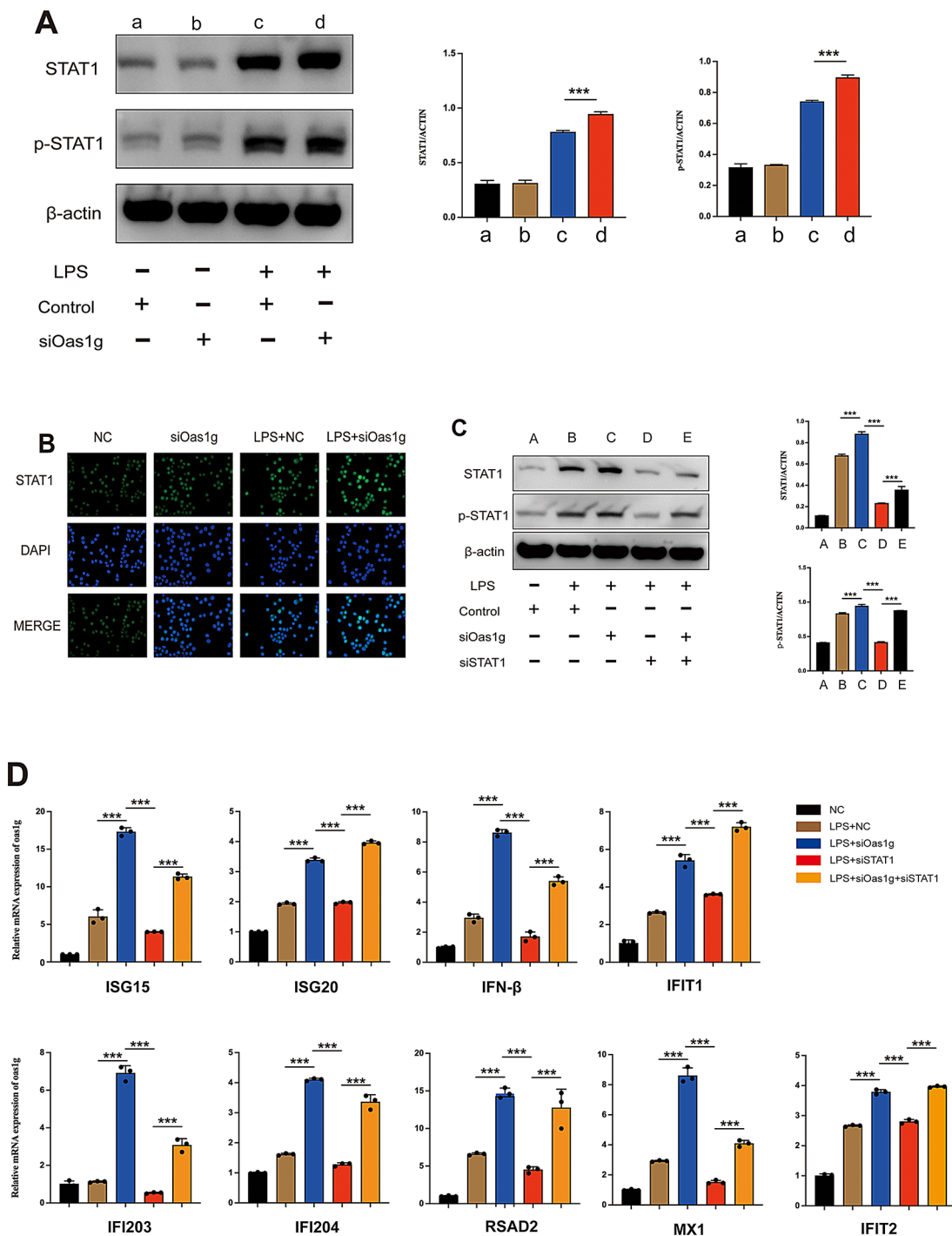


Fig. 7 Oas1g regulates ISGs via the STAT1 pathway. (A-B) After the down-regulation of Oas1g, STAT1 expression levels were detected by western blot (A) and immunofluorescence (B). (C-D) After simultaneously down-regulating Oas1g and STAT1 and treating with LPS for 24 h, the expressions of STAT1 and p-STAT1 were confirmed by western blot (C), and qRT-PCR was used to identify changes in ISGs expression in BV2 microglial cells (D). Data are expressed as mean ± SD. (* $p < 0.05$, ** $p < 0.01$, *** $p < 0.001$)

responses and ISGs significantly function in neuroinflammatory and neurodegenerative diseases involving AD, and exploring these hub ISGs further could lead to new therapeutic targets and strategies for AD treatment.

To address this need, our study aimed to uncover hub ISGs in microglia and provide a novel understanding of the pathogenesis of AD. We combined WGCNA and ML models, including SVM-RFE and LASSO, to screen the hub ISGs. Further, both in vivo and in vitro experiments

were conducted to validate the predicted results of hub ISGs. In our study, we identified *Oas1g* as a key hub ISG based on machine learning algorithms and WGCNA. Our experiments demonstrated that the expression level of *Oas1g* in the cortical region of APP/PS1/tau transgenic mice was significantly higher compared to control mice, and the expression of *Oas1g* was upregulated in LPS-stimulated microglia. These findings suggest that *Oas1g* may play a crucial role in modulating microglial activation and neuroinflammatory responses in AD.

The oligoadenylate synthase (OAS) family comprises 4 genes: OAS1, OAS2, OAS3, and OASL in humans, a group of ISGs that play a role in the 2–5 A and RNase L system [38, 39]. OAS proteins are induced by interferons (IFNs) and function as enzymes responsible for detecting exogenous nucleic acids, thereby instigating antiviral responses [40]. Upon binding to double-stranded RNA (dsRNA), OAS proteins undergo a conformational change that enables the production of 2–5 A molecules. These molecules activate RNase L, which degrades RNA to inhibit protein synthesis [39]. In the context of neuroinflammation, OAS proteins may influence the immune response by modulating RNA stability and protein synthesis in microglia.

Lin et al. demonstrated that anti-dengue activities correlate with the ability to trigger RNase L activation, and the 2'-5' OAS/RNase L system is essential for controlling Dengue virus infection [41]. Kwon et al. identified OAS1 and OAS3 as the mediators of RNase L-dependent antiviral action against HCV infection [42]. Moreover, mechanisms independent of RNase L have been reported in recent studies [40]. A study reported that flavivirus infection can be suppressed in RNase L-deficient mouse cells by *Oas1b* [43]. OAS1 is the most well-studied member of this family [44]. Human OAS1, known for its role in protection against virus infections, encompasses the combined functions of mouse *Oas1a*, *Oas1g*, and *Oas1b* [45]. Both *Oas1a* and *Oas1g* have enzymatic activity and function in enhancing IFN response via RNase L and pattern recognition receptors [45]. Therefore, investigations into *Oas1g* might advance our insights into the roles of OAS1 in the pathology of AD. A study suggested that OAS1 was screened as a risk gene significantly linked to AD in Genome-wide association studies [46]. Additionally, Magusali et al. recently identified OAS1 as a novel risk gene for AD by Genome-wide association studies and an RNA-seq transcriptome network [47]. Further, recent studies suggested that OAS1 participates in activating inflammatory responses and innate immunity responses. Huang et al. found that OAS1 and other genes of the OAS family are associated with psoriasis, and silencing them by siRNA can inhibit cell proliferation and influence the JAK-STAT pathway significantly, which may be a potential treatment for psoriasis [48]. Lee et al.

demonstrated that OAS1 downregulates the chemokines and ISGs following stimulation via TLR3 and TLR4 [49]. He et al. reported that increased levels of OAS1 are associated with the IFN- γ and IL6-JAKSTAT3 pathways in almost all cancers [50]. These findings imply that OAS1 family members, including *Oas1g*, are involved in regulating inflammatory pathways, which could be crucial in AD-related neuroinflammation.

We further explored the correlation between *Oas1g* and ISGs in LPS-induced microglial cells. LPS acts as a TLR4 agonist, activating the TLR4 signaling pathway and triggering an inflammatory response [51, 52]. In our study, silencing *Oas1g* led to a remarkable upregulation of STAT1 and representative ISGs, accompanied by a significant upregulation in the expression of IFN- β . In particular, the enrichment of the “Negative Regulation Of Type I Interferon Mediated Signaling Pathway” in GSEA suggests that *Oas1g* might inhibit excessive interferon signaling, which is aligned with our experiment. These indicate that *Oas1g* may act as a negative regulator of the IFN response in microglia, and its suppression enhances the JAK-STAT signaling pathway, leading to increased neuroinflammation.

The JAK-STAT signaling pathway is considered a classical mechanism of regulating the transcription of ISGs and consists of ligand-receptor complexes, JAKs, and STATs [53, 54]. Interferons of types I and III activate signaling pathways via TYK2 and JAK1 phosphorylation, leading to the phosphorylation and recruitment of STAT1 and STAT2, which then bind to IRF9 to form a complex known as ISGF3. Type II interferons activate signaling pathways by phosphorylating receptors via JAK1 and JAK2, leading to homodimerization and phosphorylation of STAT1. Activated STAT1 homodimers and ISGF3 migrate to the nucleus to activate the transcription of ISGs by attaching to the gamma-IFN-activated sequence or IFN-stimulated response elements, respectively [54]. Prior studies demonstrated that RNase L enhances IFN- β production via the RIG-I–MDA5–IPS-1 pathway, and transcriptional signaling is initiated by the cleavage products of cellular (self)-RNA created by RNase L [55]. However, it was based on mesenchymal cells, and further investigation is needed to understand the mechanism of how microglia regulate IFN- β and ISGs through OAS1 in neuroinflammation. Interestingly, Magusali et al. found that treatment with IFN- γ increased the expression of STAT1, and silencing OAS1 did not alter the expression of STAT1 following IFN- γ stimulation [47]. The discrepancy between our findings and those of Magusali et al. could be due to the different inflammatory stimuli used in the experiments. While Magusali et al. explored neuroinflammation under IFN- γ stimulation, which primarily activates type II interferon pathways, our study used LPS to stimulate microglia.

LPS, as a TLR4 agonist, is known to activate a broader range of interferon responses, including IFN- α and IFN- β , in addition to IFN- γ . This broader activation profile likely involves multiple signaling pathways beyond those activated by IFN- γ alone, including JAK-STAT as well as NF- κ B and MAPK pathways [56, 57]. This could explain why Oas1g knockdown in our study showed changes in ISG expression and other inflammatory markers, as Oas1g might modulate neuroinflammation through type I interferon responses rather than type II interferons like IFN- γ . Our result suggested that Oas1g act as a novel regulator that might reduce the expression level of ISGs in neuroinflammation by down-regulating the expression of STAT1 and IFN- β . This finding align with previous studies, such as Magusali et al. indicated that in human iPSC-derived microglia stimulated with IFN- γ , samples with OAS1 knocked down showed an increase in TNF- α secretion compared to samples without OAS1 silencing, suggesting that OAS1 might dampen the pro-inflammatory response [47]. Therefore, we hypothesize that OAS1 may downregulate neuroinflammatory response in AD by initially decreasing IFN- β expression, which subsequently reduces the STAT1 expression and consequently downregulates the expression of ISGs. In recent years, immunotherapy for AD has made significant advancements, gradually emerging as a promising treatment approach [58]. As the resident immune cells of the brain, microglia play a crucial role in the progression of AD through their interferon-mediated immune responses. Our study revealed that Oas1g expression is significantly elevated in microglia during AD, suggesting its potential as a novel therapeutic target. Future research can employ immunoprecipitation-mass spectrometry (IP-MS) to further investigate the specific mechanisms by which Oas1g regulates interferon-stimulated genes. Our novel insight into the role of Oas1g in microglial neuroinflammation highlights its potential as a therapeutic target, offering new avenues for modulating neuroinflammatory responses in AD.

Conclusion

The identification of Oas1g as an ISG through bioinformatics algorithms and machine learning models underscores its significance in AD. Our findings demonstrate that Oas1g is significantly upregulated in the cortical region of AD model mice and LPS-stimulated microglia, indicating its involvement in the disease process. Further investigations revealed that Oas1g modulates the inflammatory response by downregulating IFN- β and STAT1, thereby reducing the expression of ISGs in neuroinflammation. This regulatory mechanism suggests that OAS1 and its associated pathways could be promising therapeutic targets for AD. Limitations of our study include the relatively small sample

size, which can affect the statistical power and the generalizability of our findings. Overall, our study demonstrated the significance of OAS1 and its downstream pathways as prospective therapeutic targets for AD in neuroinflammation, suggesting its regulation as a promising approach for prevention and personalized treatment strategies in AD.

Supplementary Information

The online version contains supplementary material available at <https://doi.org/10.1186/s12967-025-06112-2>.

Supplementary Material 1

Acknowledgements

We thank Romero-Molina C, Sayed FA, et al. for uploading the expression profile data of high throughput sequencing. We express our gratitude to all the writers who have made valuable contributions to this work, as well as to the academic editor and reviewers for enhancing the overall quality of this article.

Author contributions

ZX, LL, YW, and YY conceptualized and designed the study. ZX, WH, ZF, LZ, and LH acquired and analyzed the data. LL, WH, ZF, and YY conducted the in vivo and in vitro experiments. ZX, LL, WH, ZF, YJ, JZ, and FW interpretate the results and drafted the manuscript. ZX, YW, and YY revised the manuscript. ZX, YW, and YY supervised the project, administered the project, and acquired funding. All authors have read and approved the final manuscript.

Funding

This study was supported by the National Natural Science Foundation of China (82101327), the Basic and Applied Basic Research Foundation of Guangdong Province (2022A1515012362), the Guangzhou Science and Technology Project (202201020111), and the Guangzhou Medical University 2023 Student Innovation Capability Improvement Program (No. 196).

Data availability

Online repositories (<https://www.ncbi.nlm.nih.gov/GEO/>) contain the datasets analyzed in this study, and their names and accession numbers can be found in the article and Supplementary Material. The raw and processed data of the microglia RNA-Seq generated in this study are deposited to the GEO database with accession number GSE261007.

Declarations

Ethics approval and consent to participate

The animal study obtained approval from the Institutional Animal Care and Use Committee of The Second Affiliated Hospital of Guangzhou Medical University (A2019-005, 6 March 2019). The study was conducted in adherence to the local legislation and institutional regulation.

Consent for publication

Not applicable.

Competing interests

The authors declare that they have no competing interests.

Author details

¹The Second Clinical Medicine School, Guangzhou Medical University, Guangzhou, China

²Department of Neurosurgery, Institute of Neuroscience, the Second Affiliated Hospital of Guangzhou Medical University, Guangzhou, China

³The Third Clinical Medicine School, Guangzhou Medical University, Guangzhou, China

⁴The Sixth Clinical Medicine School, Guangzhou Medical University, Guangzhou, China

Received: 24 May 2024 / Accepted: 8 January 2025

Published online: 14 February 2025

References

- 2024 Alzheimer's disease facts and figures. *Alzheimers Dement*. 2024;20(5):3708–821.
- Zhang XX, Tian Y, Wang ZT, Ma YH, Tan L, Yu JT. The epidemiology of Alzheimer's Disease Modifiable Risk factors and Prevention. *J Prev Alzheimers Dis*. 2021;8(3):313–21.
- Querfurth HW, LaFerla FM. Alzheimer's disease. *N Engl J Med*. 2010;362(4):329–44.
- Wang C, Shen D, Hu Y, Chen J, Liu J, Huang Y et al. Selective targeting of Class I HDAC reduces microglial inflammation in the Entorhinal Cortex of Young APP/PS1 mice. *Int J Mol Sci*. 2023;24(5).
- Heneka MT, Carson MJ, El Khoury J, Landreth GE, Brosseron F, Feinstein DL, et al. Neuroinflammation in Alzheimer's disease. *Lancet Neurol*. 2015;14(4):388–405.
- Bellenguez C, Kucukali F, Jansen IE, Kleindam L, Moreno-Grau S, Amin N, et al. New insights into the genetic etiology of Alzheimer's disease and related dementias. *Nat Genet*. 2022;54(4):412–36.
- Azam S, Haque ME, Kim IS, Choi DK. Microglial turnover in ageing-related neurodegeneration: Therapeutic Avenue to Intervene in Disease Progression. *Cells*. 2021;10(1).
- Calsolaro V, Edison P. Neuroinflammation in Alzheimer's disease: current evidence and future directions. *Alzheimers Dement*. 2016;12(6):719–32.
- Roy ER, Chiu G, Li S, Propson NE, Kanchi R, Wang B, et al. Concerted type I interferon signaling in microglia and neural cells promotes memory impairment associated with amyloid β plaques. *Immunity*. 2022;55(5):e879–e946.
- Jin M, Xu R, Wang L, Alam MM, Ma Z, Zhu S, et al. Type-I-interferon signaling drives microglial dysfunction and senescence in human iPSC models of Down syndrome and Alzheimer's disease. *Cell Stem Cell*. 2022;29(7):1135–e538.
- Olah M, Menon V, Habib N, Taga MF, Ma Y, Yung CJ, et al. Single cell RNA sequencing of human microglia uncovers a subset associated with Alzheimer's disease. *Nat Commun*. 2020;11(1):6129.
- Roy ER, Wang B, Wan YW, Chiu G, Cole A, Yin Z, et al. Type I interferon response drives neuroinflammation and synapse loss in Alzheimer disease. *J Clin Invest*. 2020;130(4):1912–30.
- Lang R, Li H, Luo X, Liu C, Zhang Y, Guo S, et al. Expression and mechanisms of interferon-stimulated genes in viral infection of the central nervous system (CNS) and neurological diseases. *Front Immunol*. 2022;13:1008072.
- Peng J, Jury EC, Dönnies P, Ciurtin C. Machine learning techniques for Personalised Medicine approaches in Immune-mediated chronic inflammatory diseases: Applications and challenges. *Front Pharmacol*. 2021;12:720694.
- Ahmed F, Kang IS, Kim KH, Asif A, Rahim CSA, Samantasinghar A, et al. Drug repurposing for viral cancers: a paradigm of machine learning, deep learning, and virtual screening-based approaches. *J Med Virol*. 2023;95(4):e28693.
- Samantasinghar A, Ahmed F, Rahim CSA, Kim KH, Kim S, Choi KH. Artificial intelligence-assisted repurposing of lubiprostone alleviates tubulointerstitial fibrosis. *Transl Res*. 2023;262:75–88.
- Ahmed F, Lee JW, Samantasinghar A, Kim YS, Kim KH, Kang IS, et al. SperoPredictor: an Integrated Machine Learning and Molecular Docking-based drug Repurposing Framework with Use Case of COVID-19. *Front Public Health*. 2022;10:902123.
- Ahmed F, Soomro AM, Chethikkattuvelli Salih AR, Samantasinghar A, Asif A, Kang IS, Choi KH. A comprehensive review of artificial intelligence and network based approaches to drug repurposing in Covid-19. *Biomed Pharmacother*. 2022;153:113350.
- Ahmed F, Yang YJ, Samantasinghar A, Kim YW, Ko JB, Choi KH. Network-based drug repurposing for HPV-associated cervical cancer. *Comput Struct Biotechnol J*. 2023;21:5186–200.
- Ahmed F, Samantasinghar A, Ali W, Choi KH. Network-based drug repurposing identifies small molecule drugs as immune checkpoint inhibitors for endometrial cancer. *Mol Divers*. 2024;28(6):3879–95.
- Tang K, Ji X, Zhou M, Deng Z, Huang Y, Zheng G, Cao Z. Rank-in: enabling integrative analysis across microarray and RNA-seq for cancer. *Nucleic Acids Res*. 2021;49(17):e99.
- Yang Y, Sun H, Zhang Y, Zhang T, Gong J, Wei Y, et al. Dimensionality reduction by UMAP reinforces sample heterogeneity analysis in bulk transcriptomic data. *Cell Rep*. 2021;36(4):109442.
- Langfelder P, Horvath S. WGCNA: an R package for weighted correlation network analysis. *BMC Bioinformatics*. 2008;9:559.
- Tibshirani R. Regression shrinkage and Selection Via the Lasso. *J Roy Stat Soc: Ser B (Methodol)*. 2018;58(1):267–88.
- Sanz H, Valim C, Vegas E, Oller JM, Reverter F. SVM-RFE: selection and visualization of the most relevant features through non-linear kernels. *BMC Bioinformatics*. 2018;19(1):432.
- Huang ML, Hung YH, Lee WM, Li RK, Jiang BR. SVM-RFE based feature selection and Taguchi parameters optimization for multiclass SVM classifier. *ScientificWorldJournal*. 2014;2014:795624.
- Shoabi M, Shah B, Ei-Sappagh S, Ali A, Ullah A, Alenezi F, et al. An advanced deep learning models-based plant disease detection: a review of recent research. *Front Plant Sci*. 2023;14:1158933.
- International AsD. World Alzheimer Report 2019: Attitudes to dementia 2019.
- Young-Pearse TL, Lee H, Hsieh YC, Chou V, Selkoe DJ. Moving beyond amyloid and tau to capture the biological heterogeneity of Alzheimer's disease. *Trends Neurosci*. 2023;46(6):426–44.
- Leng F, Edison P. Neuroinflammation and microglial activation in Alzheimer disease: where do we go from here? *Nat Rev Neurol*. 2021;17(3):157–72.
- Hong S, Beja-Glasser VF, Nfonoyim BM, Frouin A, Li S, Ramakrishnan S, et al. Complement and microglia mediate early synapse loss in Alzheimer mouse models. *Science*. 2016;352(6286):712–6.
- Weekman EM, Sudduth TL, Abner EL, Popa GJ, Mendenhall MD, Brothers HM, et al. Transition from an M1 to a mixed neuroinflammatory phenotype increases amyloid deposition in APP/PS1 transgenic mice. *J Neuroinflammation*. 2014;11:127.
- Schoggins JW. Interferon-stimulated genes: what do they all do? *Annu Rev Virol*. 2019;6(1):567–84.
- Hur JY, Frost GR, Wu X, Crump C, Pan SJ, Wong E, et al. The innate immunity protein IFITM3 modulates gamma-secretase in Alzheimer's disease. *Nature*. 2020;586(7831):735–40.
- Mattsson N, Insel P, Nosheny R, Zetterberg H, Trojanowski JQ, Shaw LM, et al. CSF protein biomarkers predicting longitudinal reduction of CSF beta-amyloid42 in cognitively healthy elders. *Transl Psychiatry*. 2013;3(8):e293.
- Zagorska A, Traves PG, Lew ED, Dransfield I, Lemke G. Diversification of TAM receptor tyrosine kinase function. *Nat Immunol*. 2014;15(10):920–8.
- Wang RG, Kaul M, Zhang DX. Interferon-stimulated gene 15 as a general marker for acute and chronic neuronal injuries. *Sheng Li Xue Bao*. 2012;64(5):577–83.
- Silverman RH. A scientific journey through the 2-5A/RNase L system. *Cytokine Growth Factor Rev*. 2007;18(5–6):381–8.
- Kristiansen H, Gad HH, Eskildsen-Larsen S, Despres P, Hartmann R. The oligoadenylate synthetase family: an ancient protein family with multiple antiviral activities. *J Interferon Cytokine Res*. 2011;31(1):41–7.
- Choi UY, Kang JS, Hwang YS, Kim YJ. Oligoadenylate synthase-like (OASL) proteins: dual functions and associations with diseases. *Exp Mol Med*. 2015;47(3):e144.
- Lin RJ, Yu HP, Chang BL, Tang WC, Liao CL, Lin YL. Distinct antiviral roles for human 2',5'-oligoadenylate synthetase family members against dengue virus infection. *J Immunol*. 2009;183(12):8035–43.
- Kwon YC, Kang JI, Hwang SB, Ahn BY. The ribonuclease L-dependent antiviral roles of human 2',5'-oligoadenylate synthetase family members against hepatitis C virus. *FEBS Lett*. 2013;587(2):156–64.
- Kajaste-Rudnitski A, Mashimo T, Frenkiel M-P, Guénet J-L, Lucas M, Despres P. The 2',5'-Oligoadenylate synthetase 1b is a potent inhibitor of West Nile Virus Replication Inside infected cells. *J Biol Chem*. 2006;281(8):4624–37.
- Fish I, Boissinot S. Functional evolution of the OAS1 viral sensor: insights from old world primates. *Infect Genet Evol*. 2016;44:341–50.
- Elkhateeb E, Tag-El-Din-Hassan HT, Sasaki N, Torigoe D, Morimatsu M, Agui T. The role of mouse 2',5'-oligoadenylate synthetase 1 paralogs. *Infect Genet Evol*. 2016;45:393–401.
- Salih DA, Bayram S, Guelfi S, Reynolds RH, Shoai M, Ryten M, et al. Genetic variability in response to amyloid beta deposition influences Alzheimer's disease risk. *Brain Commun*. 2019;1(1):fcb2022.
- Magusali N, Graham AC, Piers TM, Panichnantakul P, Yaman U, Shoai M, et al. A genetic link between risk for Alzheimer's disease and severe COVID-19 outcomes via the OAS1 gene. *Brain*. 2021;144(12):3727–41.
- Huang YZ, Zheng YX, Zhou Y, Xu F, Cui YZ, Chen XY et al. OAS1, OAS2, and OAS3 Contribute to Epidermal Keratinocyte Proliferation by Regulating

- Cell Cycle and Augmenting IFN-1–Induced Jak1–Signal Transducer and Activator of Transcription 1 Phosphorylation in Psoriasis. *J Invest Dermatol.* 2022;142(10):2635–45.e9.
49. Lee WB, Choi WY, Lee DH, Shim H, Kim-Ha J, Kim YJ. OAS1 and OAS3 negatively regulate the expression of chemokines and interferon-responsive genes in human macrophages. *BMB Rep.* 2019;52(2):133–8.
50. Yang R, Du Y, Zhang M, Liu Y, Feng H, Liu R, et al. Multi-omics analysis reveals interferon-stimulated gene OAS1 as a prognostic and immunological biomarker in pan-cancer. *Front Immunol.* 2023;14:1249731.
51. Rodríguez-Gómez JA, Kavanagh E, Engskog-Vlachos P, Engskog MKR, Herrera AJ, Espinosa-Oliva AM et al. Microglia: agents of the CNS pro-inflammatory response. *Cells.* 2020;9(7).
52. Rahimifard M, Maqbool F, Moeini-Nodeh S, Niaz K, Abdollahi M, Braidly N, et al. Targeting the TLR4 signaling pathway by polyphenols: a novel therapeutic strategy for neuroinflammation. *Ageing Res Rev.* 2017;36:11–9.
53. Hu X, Li J, Fu M, Zhao X, Wang W. The JAK/STAT signaling pathway: from bench to clinic. *Signal Transduct Target Ther.* 2021;6(1):402.
54. Wang W, Xu L, Su J, Peppelenbosch MP, Pan Q. Transcriptional regulation of Antiviral Interferon-stimulated genes. *Trends Microbiol.* 2017;25(7):573–84.
55. Malathi K, Dong B, Gale M Jr., Silverman RH. Small self-RNA generated by RNase L amplifies antiviral innate immunity. *Nature.* 2007;448(7155):816–9.
56. Ye J, Chen D, Ye Z, Huang Y, Zhang N, Lui EMK et al. Fucoidan isolated from *Saccharina Japonica* inhibits LPS-Induced inflammation in Macrophages via blocking NF-kappaB, MAPK and JAK-STAT pathways. *Mar Drugs.* 2020;18(6).
57. Qin H, Wilson CA, Lee SJ, Zhao X, Benveniste EN. LPS induces CD40 gene expression through the activation of NF-kappaB and STAT-1alpha in macrophages and microglia. *Blood.* 2005;106(9):3114–22.
58. Jin Y, Du Q, Song M, Kang R, Zhou J, Zhang H, Ding Y. Amyloid-beta-targeting immunotherapies for Alzheimer's disease. *J Control Release.* 2024;375:346–65.

Publisher's note

Springer Nature remains neutral with regard to jurisdictional claims in published maps and institutional affiliations.